Journal of Sound and Vibration 329 (2010) 1553–1569

Contents lists available at ScienceDirect

Journal of Sound and Vibration

journal homepage: www.elsevier.com/locate/jsvi

# A fast signal subspace approach for the determination of absolute levels from phased microphone array measurements

Ennes Sarradj *

*Institut Verkehrstechnik, Brandenburgische Technische Universität Cottbus, Siemens-Halske-Ring 14, 03046 Cottbus, Germany*

ARTICLE INFO

*Article history:*
Received 15 December 2008
Received in revised form
6 November 2009
Accepted 9 November 2009
Handling Editor: M.P. Cartmell
Available online 6 December 2009

ABSTRACT

Phased microphone arrays are used in a variety of applications for the estimation of acoustic source location and spectra. The popular conventional delay-and-sum beamforming methods used with such arrays suffer from inaccurate estimations of absolute source levels and in some cases also from low resolution. Deconvolution approaches such as DAMAS have better performance, but require high computational effort. A fast beamforming method is proposed that can be used in conjunction with a phased microphone array in applications with focus on the correct quantitative estimation of acoustic source spectra. This method bases on an eigenvalue decomposition of the cross spectral matrix of microphone signals and uses the eigenvalues from the signal subspace to estimate absolute source levels. The theoretical basis of the method is discussed together with an assessment of the quality of the estimation. Experimental tests using a loudspeaker setup and an airfoil trailing edge noise setup in an aeroacoustic wind tunnel show that the proposed method is robust and leads to reliable quantitative results.



## 1. Introduction

The application of phased microphone arrays has become increasingly popular in the context of acoustic testing for aeroacoustic and other applications. The phased array is used as a directional sound receiver by applying beamforming signal processing algorithms to the microphone output signals. Many applications of acoustic array measurements aim at the localization of sound sources, either on machinery and vehicles or on laboratory set-ups in the wind tunnel. Nevertheless, in many situations the estimation of reliable quantitative information about the sources is important as well. A number of different approaches are applied to calculate absolute source levels from microphone array measurements in acoustic testing.

The usual processing of array microphone output signals using conventional beamforming results in a map of sound pressure contributions. In this map, the image of a point source is a spot at the source location with dimensions that depend mainly on the wavelength of the sound and the array aperture (array dimension). This spot, corresponding to the main lobe of the array directivity, is accompanied by a number of side lobes lower in level. While localization of sound sources is still possible in many cases, these imperfections prevent the straightforward estimation of source strengths or source powers, especially if several sources are present and/or the sources are not compact, but consist of spatially extended source domains.

* Tel.: +49 355 69 4533; fax: +49 355 69 4891.
*E-mail address:* ennes.sarradj@tu-cottbus.de

0022-460X/$ - see front matter © 2009 Elsevier Ltd. All rights reserved.
doi:10.1016/j.jsv.2009.11.009

One popular approach that was successfully applied is an integration technique. Integration is performed over a source region of interest in the map. But, with the use of conventional beamforming techniques the beamforming map shows the source strength convolved with an array-dependent point spread function. This can be taken into account by integrating over a weighted beamforming map [1]. Each point in that map is weighted by an individual factor that accounts for the integrated point spread function in that point. A number of computationally less expensive approaches approximate that factor by a representative factor that does not depend on the location in the beamforming map [1–5]. Even with rigorous consideration of the point spread function, results from the integration may be influenced by contributions from outside the integration area. All integration approaches require the prior estimation of a full beamforming map.

Another class of methods uses inverse approaches for the estimation of quantitative source spectra. The spectral estimation method [6] is a parametric method. The difference between the actual cross spectral matrix of microphone signals and a theoretical cross spectral matrix is minimized. The theoretical matrix is simulated on the basis of contributions from previously defined source areas. Thus, the minimum is achieved by iteratively adjusting the source strengths. The results are quantitative source spectra, but are not unique and depend strongly on the chosen distribution of source areas. The source directivity modeling in cross spectral matrix (SODIX) [7] approach is an extension of the spectral estimation method that incorporates the directivity of the sources and was successfully applied to the noise source analysis of an aeroengine.

The deconvolution approach for the mapping of acoustic sources (DAMAS) [8] is also an inverse approach. It aims at the estimation of a ''true'' map of source strengths of uncorrelated sources. An extension (DAMAS-C) [9] of the method deals also with spatial coherence of the sources. In DAMAS, the problem is represented by a huge system of equations with as many unknowns as points in the map grid. A result can be obtained by iterative solution, but requires a large number of iterations. Other deconvolution methods [10,11] are available that make use of an approximate shift-invariant point spread function and require less computational effort. Another option for faster processing is to make use of the sparsity of the problem [12].

The CLEAN algorithm originally introduced in radio astronomy basically removes the side lobes from the beamforming map and thus makes it less ambiguous. It has been used for aeroacoustic measurements [13]. Improved variants of this algorithm, namely WB-CLEAN [14] and CLEAN-SC [15], were also applied in the context of acoustic testing.

To alleviate some of the limitations of conventional beamforming, a number of improved algorithms have been developed, mainly in the context of astro- and geophysical, radar, sonar and telecommunications applications [16,17]. Some of these methods, for example the ESPRIT [18] method, require special array geometries such as the uniform linear array and may therefore not be applied for arbitrary array geometries as used in acoustic testing. Other approaches, e.g. the minimum variance beamformer or subspace techniques, are readily applicable.

The Capon [19] or minimum variance beamformer provides a better spatial resolution than the conventional beamformer. In contrast to the latter, its actual characteristics depend on the input data and it is therefore often termed adaptive beamformer. Improved variants [20] of this beamformer were used in aeroacoustic measurements [21,22] and acoustic imaging [23]. However, the performance of these algorithms regarding estimation of absolute levels depends on the number of sources present and on the signal-to-noise ratio.

Subspace based beamforming methods rest on the general idea of separating signal and noise components. This is done using a decomposition of either the estimated covariance matrix or the cross spectral matrix of the sensor signals into a superposition of lower-rank matrices representing these components. The most prominent of these approaches is the multiple signal classification (MUSIC) algorithm [24]. In MUSIC, an eigenvalue decomposition of the cross spectral matrix separates signal and noise eigenvectors and the estimation of source position or direction of arrival is solely computed from the noise eigenvectors. Thus, amplitude information is lost entirely during the processing and no estimation of absolute source levels is possible. However, improved source localization is possible and the method was successfully applied in the context of aeroacoustic tests in a trans-sonic wind tunnel [22].

Other approaches for source localization consider the signal subspace [25,26] as well. A special variant of adaptive beamforming that bases on a cross spectral matrix reconstructed from primary signal eigenvectors was applied to multipole source localization in the case of jet noise [27]. Recently, Suzuki [28] proposed an iterative method that uses the eigenvectors from signal subspace and estimates the assigned spatial distribution of multipoles by solving an inverse problem.

In the present paper, a different method is proposed that bases on the eigenvalue decomposition of the cross spectral matrix and works in the signal subspace. It aims at the computationally efficient estimation of source strength and location. The rationale behind its development was the need for a method that allows the fast processing of data from a large number (some thousand) of single measurements. The basic idea of the method is that the individual eigenvalues and eigenvectors of the signal subspace are linked to sources or source mechanisms. Beamforming applied to data resynthesized from those eigenvectors reveals the location of such sources while the eigenvalues contain the information on the source strength.

The remainder of the paper is organized as follows: First, the theory behind the proposed method is explained. A simple model of the sound field is introduced as a basis for further mathematical development. Then, the conventional beamformer is put into the context of that model and the DAMAS approach is briefly introduced. Next, the eigenvalue decomposition of the cross spectral matrix is analyzed and an approximation for the source strength on the basis of this decomposition is introduced. Error bounds for this approximation are derived and the procedure of sound source

localization using a modified beamformer is explained. Afterwards, the setup of two dedicated experiments for the test of the proposed method is presented. Then, the possible error of the results is examined using a Monte-Carlo approach and the results from the experiments are presented and compared to DAMAS results. Finally, the computational requirements are discussed and the advantages and limitations of the proposed method are highlighted.

## 2. Theory

### 2.1. Sound field model

An array of $N$ microphones is used for analysis. In the presence of a single sound source, the complex-valued sound pressure $p$ at the $i$-th microphone at $\mathbf{x}_i$ is

$$p(\mathbf{x}_i) = a(\mathbf{x}_i, \mathbf{x}_0, \mathbf{x}_s) q(\mathbf{x}_s), \tag{1}$$

where $q$ is the sound pressure at an arbitrary reference location $\mathbf{x}_0$ due to that source. For convenience, this reference location may be chosen to be the center of the array. The transfer function $a$ depends on the type of the source, its location $\mathbf{x}_s$ and the environmental conditions. In case of a point source, the transfer function is given by the appropriate Green's function $G$:

$$a(\mathbf{x}_i, \mathbf{x}_0, \mathbf{x}_s) = \frac{G(\mathbf{x}_i, \mathbf{x}_s)}{G(\mathbf{x}_0, \mathbf{x}_s)}. \tag{2}$$

This Green's function can be estimated for a number of scenarios, including flow and shear layers [29]. In the absence of any flow and reflecting boundaries, the result for a free sound field is

$$a(\mathbf{x}_i, \mathbf{x}_0, \mathbf{x}_s) = \frac{r_0}{r_i} \mathrm{e}^{-\mathrm{j}k(r_i - r_0)}, \tag{3}$$

with $r_i = |\mathbf{x}_s - \mathbf{x}_i|$ and $r_0 = |\mathbf{x}_s - \mathbf{x}_0|$ indicating the distance between the source and the microphone location and the distance between the source and the reference location, respectively. The vector of sound pressures at the microphones due to a source at $\mathbf{x}_s$ is given by $\mathbf{p} = \mathbf{a}(\mathbf{x}_0, \mathbf{x}_s) q(\mathbf{x}_s)$. The transfer vector $\mathbf{a}(\mathbf{x}_0, \mathbf{x}_s)$ contains all respective transfer functions.

Any realistic sound field is composed of contributions from several sources. Therefore, it can be modeled as a superposition of sound fields due to several sound sources and source mechanisms. The sound pressure at any microphone is then also a superposition of contributions from several sound sources. In practice, additional noise will be present. This noise is mostly not of acoustic origin but comes from non-acoustic pressure fluctuations due to flow and from the microphone electronics and data acquisition. It is unrelated to any of the sound sources and is represented by the elements of $\mathbf{n}$. For $M$ sources, the sound pressures at the microphones are thus given by

$$\mathbf{p} = \mathbf{A}\mathbf{q} + \mathbf{n}, \tag{4}$$

where the $N$-by-$M$ matrix $\mathbf{A}$ contains the transfer functions as its elements. The columns of this matrix are the transfer vectors $\mathbf{a}_j$ that belong to the sources. The signal $q_j$ of any sound source is assumed to be uncorrelated to any noise signal $n_i$. Thus, the cross spectrum $E\{q_j n_i^*\}$ is zero and the matrix of cross spectrum elements of the microphone signals is given by

$$E\{\mathbf{p}\mathbf{p}^{\mathrm{H}}\} = \mathbf{A}E\{\mathbf{q}\mathbf{q}^{\mathrm{H}}\}\mathbf{A}^* + E\{\mathbf{n}\mathbf{n}^{\mathrm{H}}\}, \tag{5}$$

where $E\{\}$ denotes the expectation operator and the superscript H indicates the conjugate transpose. Under the assumption that all noise signals are of equal amplitude $n$ and are mutually uncorrelated, this simplifies to

$$\mathbf{G} = \mathbf{A}\mathbf{S}\mathbf{A}^{\mathrm{H}} + n^2\mathbf{I}, \tag{6}$$

with $\mathbf{G}$ and $\mathbf{S}$ denoting the cross spectral matrices of the microphone signals and of the source signals, respectively, and $\mathbf{I}$ denoting the identity matrix. Eq. (6) provides a useful model for the sound field that can be used as a basis for both localization of sound sources and estimation of source strengths.

### 2.2. Conventional beamforming

Because all quantitative information about the sources is contained in the cross spectral matrix of source signals $\mathbf{S}$, the problem of estimating the source strengths is equivalent to the estimation of that matrix. For $M \leq N$, the sound field model in Eq. (6) can be transformed to give

$$\mathbf{S} = \mathbf{A}^{+}(\mathbf{G} - n^2\mathbf{I})\mathbf{A}^{\mathrm{H}^{+}}, \tag{7}$$

where $^+$ indicates the Moore–Penrose pseudoinverse [30]. In order to estimate $\mathbf{S}$ using this equation, the transfer matrix $\mathbf{A}$ must be known. Therefore, the source locations must be found in order to get the transfer vectors contained in that matrix. As it is difficult to get a fully correct estimate for these vectors, the direct application of Eq. (7) for source estimation cannot be expected to yield good results in practice. Moreover, the model is not applicable if there are more sources than

microphones. If only one single source is considered, Eq. (7) simplifies to give

$$S = \frac{\mathbf{a}(\mathbf{x}_s)^{\mathrm{H}}}{\mathbf{a}(\mathbf{x}_s)^{\mathrm{H}}\mathbf{a}(\mathbf{x}_s)}(\mathbf{G} - n^2\mathbf{I})\frac{\mathbf{a}(\mathbf{x}_s)}{\mathbf{a}(\mathbf{x}_s)^{\mathrm{H}}\mathbf{a}(\mathbf{x}_s)}. \tag{8}$$

This equation is equivalent to a spatial filter commonly known as the conventional delay-and-sum beamformer. For an arbitrary position $\mathbf{x}_t$, the output of such a filter is the sum of the microphone signals weighted by the elements of the steering vector $\mathbf{h}$ with $\mathbf{h}^{\mathrm{H}}(\mathbf{x}_t)\mathbf{a}(\mathbf{x}_t) = 1$:

$$p_F(\mathbf{x}_t) = \mathbf{h}(\mathbf{x}_t)^{\mathrm{H}}\mathbf{p}. \tag{9}$$

The auto power spectrum $B$ of the filter output is

$$B(\mathbf{x}_t) = E\{p_F(\mathbf{x}_t)p_F^*(\mathbf{x}_t)\} = \mathbf{h}^{\mathrm{H}}(\mathbf{x}_t)\mathbf{G}\mathbf{h}(\mathbf{x}_t). \tag{10}$$

This spatial filter lets pass the signal from a source at $\mathbf{x}_t$ unattenuated. A simple model for the unwanted sound is to assume that this is impinging from any other location at the same time with same power. These spatially white signals [31] are attenuated as much as possible, if

$$\mathbf{h} = \frac{\mathbf{a}(\mathbf{x}_t)}{\mathbf{a}(\mathbf{x}_t)^{\mathrm{H}}\mathbf{a}(\mathbf{x}_t)} \tag{11}$$

is chosen. This choice for the steering vector is equivalent to the formulation in Eq. (8). In the sound field model (3) a point source in a free sound field was considered. Thus, the elements of $\mathbf{h}$ are given by

$$h_i = \frac{1}{r_0 r_i \sum_{j=1}^{N}\frac{1}{r_j^2}}\mathrm{e}^{-\mathrm{j}k(r_i - r_0)}. \tag{12}$$

Since the available measurement sample is always of finite length, the true cross spectral matrix of microphone signals $\mathbf{G}$ must be replaced by an estimate $\hat{\mathbf{G}}$ of that matrix. With this estimate, the peaks of the function

$$B(\mathbf{x}_t) = \mathbf{h}(\mathbf{x}_t)^{\mathrm{H}}\hat{\mathbf{G}}\mathbf{h}(\mathbf{x}_t) \tag{13}$$

can be used to approximate the location and power of sound sources. As can be seen by comparison with Eq. (8), the influence of the noise that occurs in $\hat{\mathbf{G}}$ can be eliminated by removing the main diagonal from that matrix. However, such diagonal removal will have some unpredictable influence on the absolute value of $B$.

In the presence of one single source, the beamformer output power $B$ is at maximum if $x_t = x_s$. Moreover, $B$ is a good estimation of the source power $S = qq^*$ in this case. If more than one source is present, the quality of the estimation depends on the beamformer characteristics and therefore on the source locations, the frequency and the number and layout of the microphones in the array. Especially for frequencies with wavelengths not small compared to the array aperture or for sources close to each other, the estimate of source location and power may be wrong. This limits the usefulness of the conventional beamformer for the estimation of source strengths.

A possible solution arises when the beamformer is interpreted as an imaging system that maps a source distribution $S(\mathbf{x}_s)$ to an image $B(\mathbf{x}_t)$ via a point spread function $P(\mathbf{x}_s, \mathbf{x}_t)$:

$$B(\mathbf{x}_t) = \sum_{\mathbf{x}_s} P(\mathbf{x}_s, \mathbf{x}_t)S(\mathbf{x}_s) \quad \text{for each} \quad \mathbf{x}_t. \tag{14}$$

Under the assumption of incoherent sources the unknown source distribution can be calculated from the known beamformer result and from the point spread function via the DAMAS [8] deconvolution method, where the system of equations (14) is solved with a special iterative technique. The contribution from source domains may be quantitatively characterized by spatial integration of a region of the source distribution. This is a robust approach that is known to yield reliable results in many practical situations where the assumption of incoherent sources is justified. It is, however, very expensive in terms of calculation time.

### 2.3. Eigenvalue decomposition and orthogonal beamforming

Cross spectral matrices are Hermitian and positive semidefinite. Thus, the eigenvalue decomposition of the cross spectral matrix of microphone signals is

$$\mathbf{G} = \mathbf{V}\mathbf{\Lambda}\mathbf{V}^{\mathrm{H}}, \tag{15}$$

where $\mathbf{\Lambda}$ is a diagonal matrix with the positive real-valued eigenvalues of $\mathbf{G}$ and the matrix $\mathbf{V}$ holds the respective eigenvectors.

Following Su and Morf [26], it shall be assumed here that the $N - M$ smallest eigenvalues are all equal to $n^2$ and the eigenvalue decomposition can be split into two parts:

$$\mathbf{G} = \mathbf{V}\begin{bmatrix}\mathbf{\Lambda}_S & 0\\ 0 & 0\end{bmatrix}\mathbf{V}^{\mathrm{H}} + n^2\mathbf{V}\mathbf{V}^{\mathrm{H}} = \mathbf{V}_S\mathbf{\Lambda}_S\mathbf{V}_S^{\mathrm{H}} + n^2\mathbf{I}, \tag{16}$$

where

$$\mathbf{\Lambda} = \begin{bmatrix} \mathbf{\Lambda}_S + n^2\mathbf{I} & 0 \\ 0 & n^2\mathbf{I} \end{bmatrix}. \tag{17}$$

The first of these parts corresponds to the source signals while the second one corresponds to the noise. Accordingly, the eigenvectors in $\mathbf{V}_S$ span the signal subspace of $\mathbf{V}$ and the remaining eigenvectors span the noise subspace. In a practical experiment, the eigenvalues connected with the noise subspace may be not equal, but as long as they are much smaller than the signal subspace eigenvalues, this will have only minor influence on the signal subspace eigenvalues and eigenvectors.

The comparison of Eqs. (6) and (16) leads to the eigenvalue decomposition

$$\mathbf{ASA}^{\mathrm{H}} = \mathbf{V}_S \mathbf{\Lambda}_S \mathbf{V}_S^{\mathrm{H}}. \tag{18}$$

This equation is multiplied by $\mathbf{A}^{\mathrm{H}}$ on the left and by $\mathbf{A}^{\mathrm{H}^+}$ on the right to yield

$$\mathbf{A}^{\mathrm{H}}\mathbf{AS} = \mathbf{A}^{\mathrm{H}}\mathbf{V}_S \mathbf{\Lambda}_S \mathbf{V}_S^{\mathrm{H}} \mathbf{A}^{\mathrm{H}^+}. \tag{19}$$

Note that both $\mathbf{A}$ and $\mathbf{V}_S$ are $N$-by-$M$ matrices. The matrix $\mathbf{V}$ is unitary and therefore $\mathbf{V}_S^{\mathrm{H}} = \mathbf{V}_S^{+}$. Making use of the relation $(\mathbf{A}^{\mathrm{H}}\mathbf{V}_S)^{-1} = \mathbf{V}_S^{\mathrm{H}}\mathbf{A}^{\mathrm{H}^+}$ Eq. (19) can be also written as

$$(\mathbf{A}^{\mathrm{H}}\mathbf{A})\mathbf{S} = (\mathbf{A}^{\mathrm{H}}\mathbf{V}_S)\mathbf{\Lambda}_S(\mathbf{A}^{\mathrm{H}}\mathbf{V}_S)^{-1}. \tag{20}$$

It becomes clear that $\mathbf{\Lambda}_S$ and $(\mathbf{A}^{\mathrm{H}}\mathbf{A})\mathbf{S}$ are similar matrices and share their eigenvalues. Thus, the eigenvalues of the matrix $(\mathbf{A}^{\mathrm{H}}\mathbf{A})\mathbf{S}$ are the same as the $M$ largest eigenvalues $\Lambda_{Sii}$ of the microphone signal cross spectral matrix. Furthermore, the eigenvalues can be used to approximate the source strengths. This approximation shall now be discussed in more detail.

If the Hermitian matrix $\mathbf{H} = \mathbf{A}^{\mathrm{H}}\mathbf{A}$ is introduced, the left-hand side of Eq. (20) can be written as $\mathbf{C} = \mathbf{HS}$. The entries of $\mathbf{H}$ are

$$H_{ij} = \mathbf{a}_i^{\mathrm{H}}\mathbf{a}_j = r_{0i}r_{0j}\sum_{l=1}^{N}\frac{\mathrm{e}^{-\mathrm{j}k(r_{lj}-r_{li})}}{r_{lj}r_{li}}, \tag{21}$$

where $\mathbf{a}_i$ and $\mathbf{a}_j$, given by Eq. (3), are the vectors of transfer functions that correspond to source $i$ and to source $j$, respectively.

For off-diagonal entries the distances $r_{lj}$ and $r_{li}$ are generally different and the summation is over complex numbers with similar magnitude, but different phase. Thus, the absolute value of the off-diagonal entries of $\mathbf{H}$ tends to be smaller than that of the real-valued main diagonal entries where always $\mathrm{e}^{-\mathrm{j}k(r_{lj}-r_{li})} = 1$. While from (21) only the mild condition $|H_{ij}| < \max(H_{ii}, H_{jj})$ is strictly true, for sufficiently different $\mathbf{a}_i$ and $\mathbf{a}_j$ the absolute values of the off-diagonal entries are much smaller than the diagonal entries of the same row or column.

If all sources are assumed to be uncorrelated, $\mathbf{S}$ is a diagonal matrix and its eigenvalues are the diagonal entries and correspond to the source powers $S_{ii} = q_i q_i^*$. The elements of $\mathbf{C}$ are

$$C_{ij} = H_{ij}S_{ii}. \tag{22}$$

Further, from the equality of the traces of $\mathbf{C}$ and $\mathbf{\Lambda}$ it follows that the sum of eigenvalues is equal to the weighted sum of source strengths

$$\sum_{i=1}^{M} H_{ii}S_{ii} = \sum_{i=1}^{M} \Lambda_{Sii}. \tag{23}$$

This equation suggests the following approximation for the individual source powers:

$$S_{ii} \approx \frac{\Lambda_{Sii}}{H_{ii}}. \tag{24}$$

The relative error of this approximation may be defined as

$$e_i = \frac{\left| S_{ii} - \dfrac{\Lambda_{Sii}}{H_{ii}} \right|}{S_{ii}}. \tag{25}$$

The Gershgorin circle theorem [32] and its corollaries [33] may be used to establish mathematical bounds for this error. These bounds can be given either in terms of absolute column sums or of absolute row sums of the off-diagonal matrix entries of $\mathbf{C}$:

$$e_i \le \frac{1}{C_{ii}}\sum_{\substack{j=1 \\ j\neq i}}^{M} |C_{ji}| = \frac{1}{H_{ii}}\sum_{\substack{j=1 \\ j\neq i}}^{M} |H_{ji}|, \tag{26}$$

$$e_i \le \frac{1}{C_{ii}} \sum_{\substack{j=1 \\ j \neq i}}^{M} |C_{ij}| = \frac{1}{H_{ii}} \sum_{\substack{j=1 \\ j \neq i}}^{M} \frac{S_{jj}}{S_{ii}} |H_{ji}|. \tag{27}$$

From (26) it becomes clear that the error depends on the absolute values of the off-diagonal entries of **H** compared to the diagonal entry in the same column. As discussed above, this depends on the vectors of transfer functions for the individual sources and thus on the wave number $k$, the number of microphones $N$ and the range of possible $r_{li} - r_{lj}$, which is governed by the spacing of the sources $i$ and $j$. The error bound tends to become smaller with increasing wave number, number of microphones and source spacing.

An additional conclusion may be drawn from (27). If the power of source $i$ is larger than that of source $j$, then $S_{jj}/S_{ii} < 1$ and the error for source $i$ will decrease. This suggests that a larger spacing of the eigenvalues results in a better quality of the approximation. Using some examples, the error bounds given can be found to be rather broad. However, in a practical situation the actual errors of the approximation may be much smaller. The results of the Monte Carlo simulation given in Section 4.1 indeed indicate considerably small errors, mostly less than 1 dB.

The use of Eq. (24) to approximate the source strengths from the eigenvalues requires $H_{ii}$ and thus the knowledge of the source position is necessary. However, it is possible to use the approximation without knowing the source position. If the reference location $\mathbf{x}_0$ is in the array center, then from Eq. (22) it can be seen that

$$H_{ii} = \sum_{l=1}^{N} \frac{r_{0i}^2}{r_{li}^2} \approx N. \tag{28}$$

This approximation is also often implicitly used in the literature on acoustical beamforming (e.g. [34]) to replace $\mathbf{a}(\mathbf{x}_t)^{\mathrm{H}}\mathbf{a}(\mathbf{x}_t)$ in (11) by $N$. Eqs. (24) and (28) can be used together to estimate the source strength without beamforming. In this case, the computational effort is limited to an eigendecomposition of the cross spectral matrix **G**.

However, for the application in acoustic testing the location of the sources is also of interest. From the full beamforming result these locations are not always obvious because not all peaks in the beamforming map from (13) correspond to sources. Moreover, it is not easily possible to assign the peaks to the respective source strengths from (24). The following approach using a modified beamformer allows to map the eigenvalues to specific locations. From each eigenvalue $\Lambda_{Sii}$ and the appropriate eigenvector $\mathbf{v}_i$ a component $\mathbf{G}_i = \mathbf{v}_i \Lambda_{Sii} \mathbf{v}_i^{\mathrm{H}}$ of the decomposed cross spectral matrix can be calculated. The modified beamformer uses these components to construct one beamforming map for each eigenvalue:

$$B_i(\mathbf{x}_t) = \mathbf{h}(\mathbf{x}_t)^{\mathrm{H}} \mathbf{G}_i \mathbf{h}(\mathbf{x}_t). \tag{29}$$

This map is the output of the spatial beamforming filter for only one single source. Thus, the highest peak in this map is an estimate of the source location $x_s$. As for the full beamformer, the main diagonal of $\mathbf{G}_i$ may be removed to eliminate the influence of noise in the beamforming map. In contrast to the full beamformer (13), the calculation of the map for one component can be done very efficiently using single summation:

$$B_i(\mathbf{x}_t) = \Lambda_{Sii} \sum_{j=1}^{N} (|h_j(\mathbf{x}_t)^* v_{ij}|^2 - |h_j(\mathbf{x}_t)|^2 |v_{ij}|^2). \tag{30}$$

On the basis of this results, a new method is proposed for the combined estimation of location and strength of sound sources. As the orthogonality of the eigenvectors is essential to the method, it is suggested here to identify it as orthogonal beamforming (OB). The computational procedure for this method starts with the estimated cross spectral matrix. Then, the calculation of eigenvalues and eigenvectors and the estimation of $M$ different beamforming maps using (29) follows. The number of sources $M$ may be either guessed or it may be assessed using statistical criteria that may be calculated on the basis of the estimated eigenvalues. One example of such a method was given by Wax and Kailath [35].

Finally, each of the $M$ largest eigenvalues is assigned to the location of the highest peak in the respective map. Thus, both location and strength of the apparent sources are estimated and can be used to plot a map. This map will have no more than $M$ entries that are different from zero. Often the contribution from a certain source region or sector of the map is of interest. This contribution can be calculated by taking the sum of all eigenvalues that have their corresponding peaks in the beamforming map within this region. This procedure is equivalent to the integration over that region in the map.

## 3. Experimental applications

Two different experimental setups were chosen to analyze the properties of the proposed method. The first experiment includes a laboratory setup of four small loudspeakers for validation purposes, while the second is aiming at the more practical task of airfoil trailing edge noise measurement.

The four loudspeaker experiment is designed with the intention that conventional beamforming would provide no good separation between the sound sources nor reliable quantitative information about the sources in this case. Within a quiet, but not anechoic laboratory environment, the nominally identical loudspeakers were placed at the corners of a square with an edge length of 10 cm. An array of 56 microphones was installed in a distance of 78 cm from the plane of the loudspeaker arrangement. The microphones were flush-mounted into a square aluminum plate of 1.5 m × 1.5 m. The microphone

mounting holes were milled using a computer numeric controlled milling machine assuring an accuracy of at least 0.1 mm. Fig. 1 shows both the microphone layout and the loudspeakers A, B, C and D.

The loudspeakers were driven with white noise signals. The amplitude of each of these signals was initially adjusted to result in an A-weighted sound pressure level of 90 dB in the array center if only one loudspeaker was operated. Following this calibration procedure, measurements were performed for four different test configurations.

In the first configuration, each of the four loudspeakers produced approximately the same sound pressure level in the array center. To this end, all four loudspeakers were driven with uncorrelated white noise signals at the calibrated amplitudes. In the second configuration, noise signals with different amplitudes were used. The level at loudspeaker A was left unaltered, while the driving signal levels at loudspeakers B, C and D were set to −3, −6 and −9 dB, respectively. In the third configuration, the level differences were doubled to −6, −12 and −18 dB. Finally, only loudspeaker A was driven at the same amplitude that was used in all other configurations and the other loudspeakers were switched off. Table 1 summarizes the parameters for the test configurations.

The output signals of the microphones were sampled and digitized using 24-bit data acquisition hardware and a sampling rate of 51.2 kHz. For every channel, an FFT with prior von Hann weighting was applied to 1000 consecutive, 50 percent overlapping blocks of 4096 samples each. Then, all $56^2$ cross spectra were calculated and averaged over the 1000 blocks to produce the cross spectral matrix. The conventional beamformer (CB), the proposed OB method as well as DAMAS were applied using this cross spectral matrix for a frequency range of 562.5 Hz up to 22437.5 Hz. This range covers all spectral lines within the third octave bands from 630 Hz to 20 kHz. The map grid used for all methods is 40 cm × 40 cm with 1 cm spacing and an overall number of grid points of 1681.

The airfoil trailing edge noise experiment was set up in the aeroacoustic wind tunnel [36] at Brandenburg University of Technology in Cottbus. This wind tunnel was used in a configuration with an open jet of 20 cm diameter at a wind speed of 52 m/s ($M = 0.15$). An SD 7003 airfoil with a chord length of 235 mm and a blunt trailing edge of 0.5 mm thickness was placed at 0° angle of attack in the jet as shown in Fig. 2. To trip the boundary layer, 0.15 mm tape was used at 10.6 percent

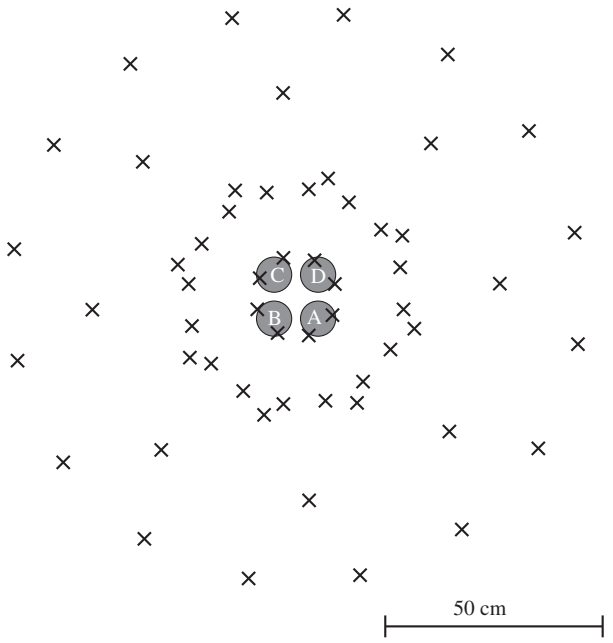


**Fig. 1.** Schematic representation of the test set-up: A, B, C, and D denote the positions of the loudspeakers at the vertexes of a 10 cm × 10 cm square, the × symbols denote positions of the array microphones in a plane 78 cm distant from the loudspeakers.

**Table 1**
Test configurations: level difference $\Delta L$ and signal levels $L$ of all loudspeakers relative to loudspeaker A.

| Configuration | $\Delta L$ (dB) | $L_A$ (dB) | $L_B$ (dB) | $L_C$ (dB) | $L_D$ (dB) |
|---|---|---|---|---|---|
| 1 | 0 | 0 | 0 | 0 | 0 |
| 2 | 3 | 0 | −3 | −6 | −9 |
| 3 | 6 | 0 | −6 | −12 | −18 |
| 4 | – | 0 | – | – | – |

chord length at both sides of the airfoil. The same 56-microphone array as for the first experiment was used with the array plane in a distance of 0.68 m parallel to the trailing edge and to the axis of the wind tunnel nozzle. The signal processing was similar to the four loudspeaker experiment. The map grid covers 60 cm × 60 cm with 2 cm spacing and has an overall number of grid points of 961. A sector of 10 cm × 16 cm at the trailing edge defines the source region.

## 4. Results and discussion

### 4.1. Quality of approximation

The proposed orthogonal beamforming (OB) method uses the approximation (24) for the source strength. The quality of this approximation is given by the error defined in Eq. (25). If the source positions and source strengths are known, this error can be calculated for any specific setup from the matrix of transfer functions **A** and the source cross spectral matrix **S**.

In case of the four loudspeaker setup, four sources must be considered. The mean approximation error for the amplitude of these sources is plotted in Fig. 3 for the different configurations from Table 1. The error depends on frequency and is in the order of 1 dB for frequencies above 1.25 kHz. Moreover, the error depends on the level difference between the sources. It becomes smaller for higher level differences. This is in agreement with the trend of the theoretical estimation (27) of the error bound also shown in Fig. 3. However, the actual error is much smaller than the predicted error bound.

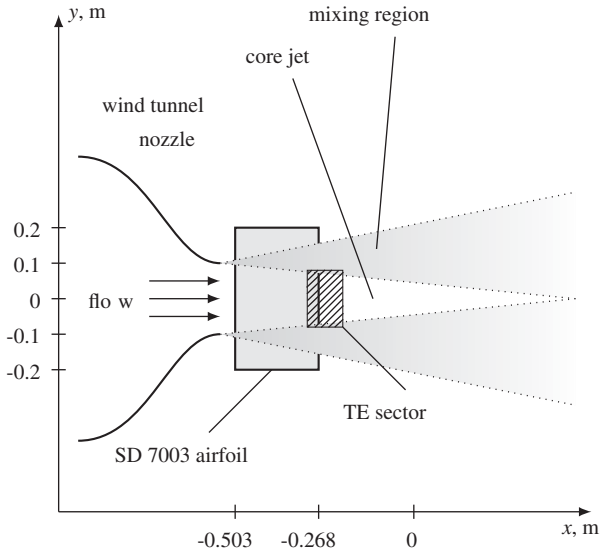


**Fig. 2.** Experimental setup in the aeroacoustic wind tunnel.

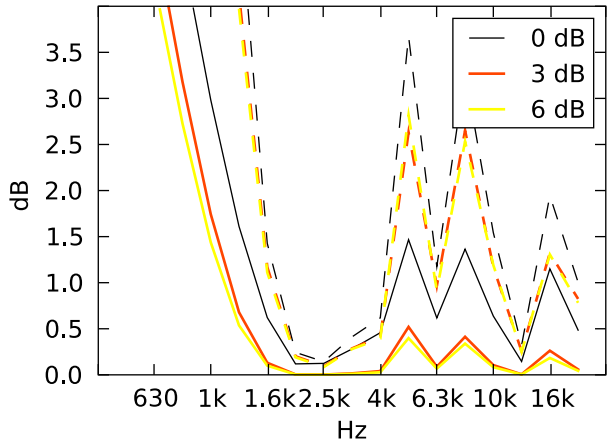


**Fig. 3.** Estimated mean approximation error (solid line) and theoretical error bound (dashed line) for level differences of 0, 3 and 6 dB between the loudspeakers in the four loudspeaker setup.

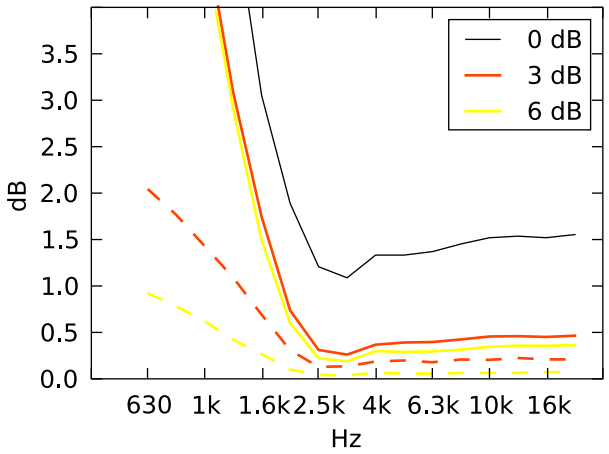


**Fig. 4.** Result of the Monte Carlo simulation: score of the 90%-percentile of the error for level differences of 0, 3 and 6 dB between the sources, solid line: mean of four sources, dashed line: source with highest amplitude.

In practice neither the source positions or the source strengths will be known prior to a measurement. Thus, only a statistical approach offers some insight into the possible errors of the approximation before a measurement. On the basis of the parameters of the four loudspeaker setup, a Monte Carlo simulation was used to calculate the errors for 10 000 different setups of four sources. The sources were placed at random positions on a 50 cm × 50 cm plane 78 cm in front of the microphone array, but had a minimum distance of 10 cm between each other. Fig. 4 shows the 90%-percentile of the mean error for the four sources. Again, the error becomes smaller for higher frequencies and for larger level differences of the sources. The error of the source with the highest amplitude is smaller than the mean error. The results of the Monte Carlo simulation indicate that the method will have a small approximation error in the order of 1 dB for frequencies above 2 kHz.

### 4.2. Four loudspeakers

The results from the proposed OB method shall be compared here with those from the conventional beamformer (CB) and from the DAMAS approach. CB is a standard technique, but offers limited capabilities for source strength estimation. DAMAS is considered here as a robust method that yields reliable results and can serve as a benchmark.

Fig. 5 shows beamforming maps for the four-loudspeaker experiment with equal signal levels (configuration 1 in Table 1). The CB results are calculated using a cross spectral matrix with the diagonal removed. Any negative results in the map that appear as a consequence from the diagonal removal are set to zero. While usually less iterations will suffice, DAMAS is performed with 5000 iterations to provide a solution that has definitely converged. Four sources are expected to be found in the measurement result. Thus, OB calculations need to consider the four largest eigenvalues. However, in practical measurements with an unknown number of sources, this information is not available and the number of sources must be assessed. In view of this consideration two different OB calculations were done, using the 20 largest eigenvalues and the six largest eigenvalues.

The beamforming maps are shown for two different frequencies that were chosen to render the CB result for the test configuration ambiguous. At 2 kHz, the CB suffers from low resolution with a main lobe width of 7 cm and the loudspeaker sources cannot be separated in the map. At 15 kHz, the sources are not clearly distinguishable from the high side lobes that are present in the CB map. The DAMAS results show the sound sources at their respective positions, but for 2 kHz a fifth, spurious source is present in the map for unknown reasons. As expected, all four source levels appear to be similar in the DAMAS results. The OB result shows four sources for both frequencies, but the source positions are imprecise for 2 kHz and the source levels are not exactly the same.

For the second test configuration (Fig. 6), the quality of the results is similar. The CB maps do not allow a proper identification of source positions or of the different source levels. The DAMAS results show the position as well as the different source levels, but also a spurious source at both 2 and 15 kHz. For 2 kHz, source positions are inaccurate with OB. However, the OB result maps indicate different levels of the four sources as desired. The third configuration (Fig. 7) has a nominal level difference between loudspeakers A and D as high as 18 dB. In this case, DAMAS unexpectedly fails to detect the minor source (loudspeaker D) for both 2 and 15 kHz. The OB result, however, shows four sources at both frequencies and also a greater level difference compared to the second test configuration. It appears that a scenario with sources of various strengths poses a problem for the DAMAS approach while according to the results from Section 4.1 it is favorable when OB is applied.

The beamforming maps allow the estimation of result quality at single frequencies only. To demonstrate the performance of the proposed method for a larger frequency range, the source spectra from OB are benchmarked here

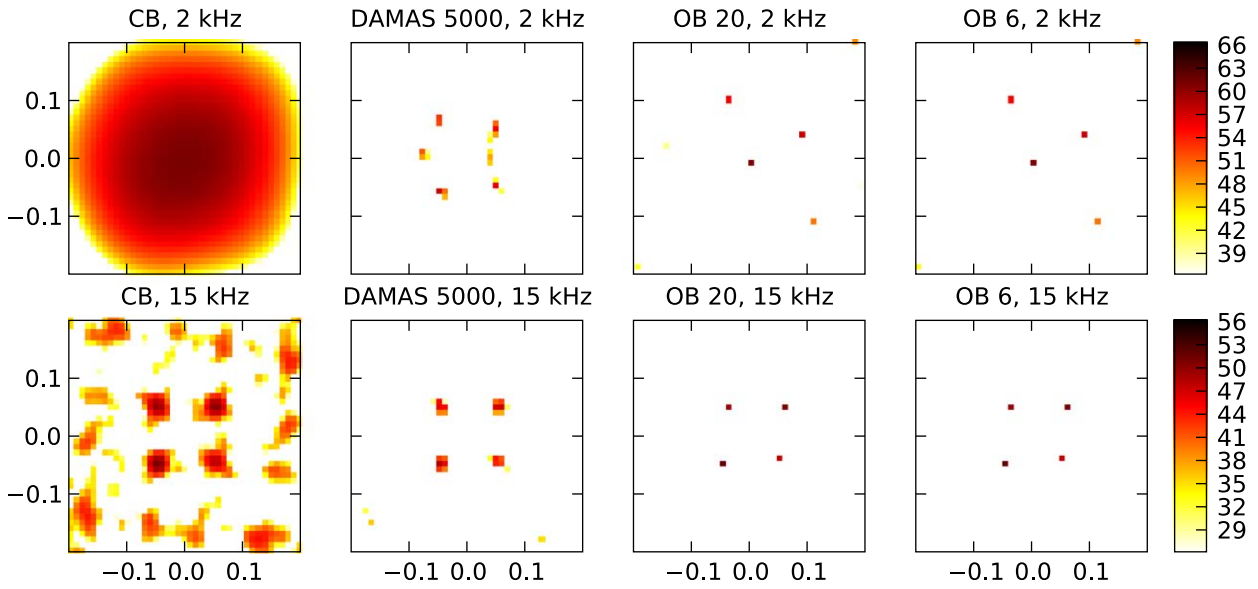


**Fig. 5.** Maps of narrow band sound pressure level in dB in the array center for configuration 1 from Table 1, dimensions are in m, results from conventional beamforming (CB), the deconvolution approach for the mapping of acoustic sources (DAMAS) using 5000 iterations and orthogonal beamforming (OB) using the 6 and the 20 largest eigenvalues, true locations of the sources: (0.05, −0.05 m) for A, (−0.05, −0.05 m) for B, (−0.05, 0.05 m) for C, and (0.05, 0.05 m) for D.

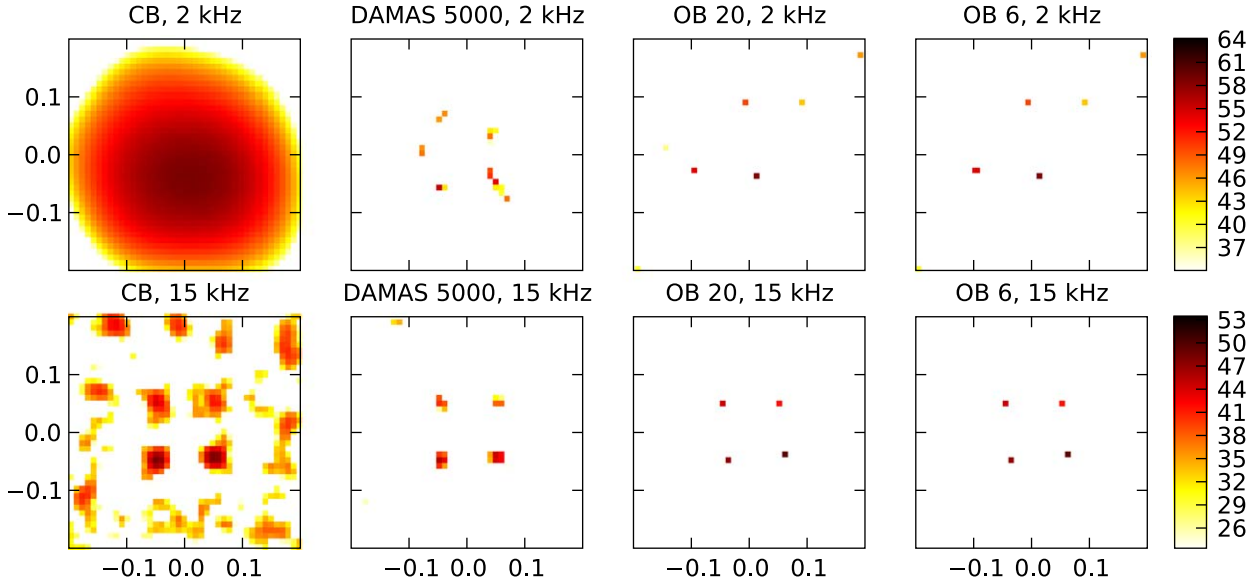


**Fig. 6.** Maps of sound pressure level as in Fig. 5, but for configuration 2 from Table 1.

against the spectra from DAMAS. CB results for spectra are omitted. For DAMAS, such spectra were recovered by integration over four sectors of 10 cm × 10 cm that are defined in the map grid around the position of the loudspeakers. For the OB method, the same sectors are used as the source region to decide whether an eigenvalue contributes to a specific source. If the maximum of the map that corresponds to an eigenvalue was located inside one sector that eigenvalue was considered to contribute to the respective source.

For the first test configuration in Figs. 8(a) and (b), both methods show comparably good results in the frequency range above 2 kHz. At lower frequencies, OB estimates the apparent location of the sources to be outside the sectors. Consequently, no eigenvalue is found to contribute to the source. Thus, the source strength for the respective source is zero. A similar behavior can also be observed at a few higher frequency lines.

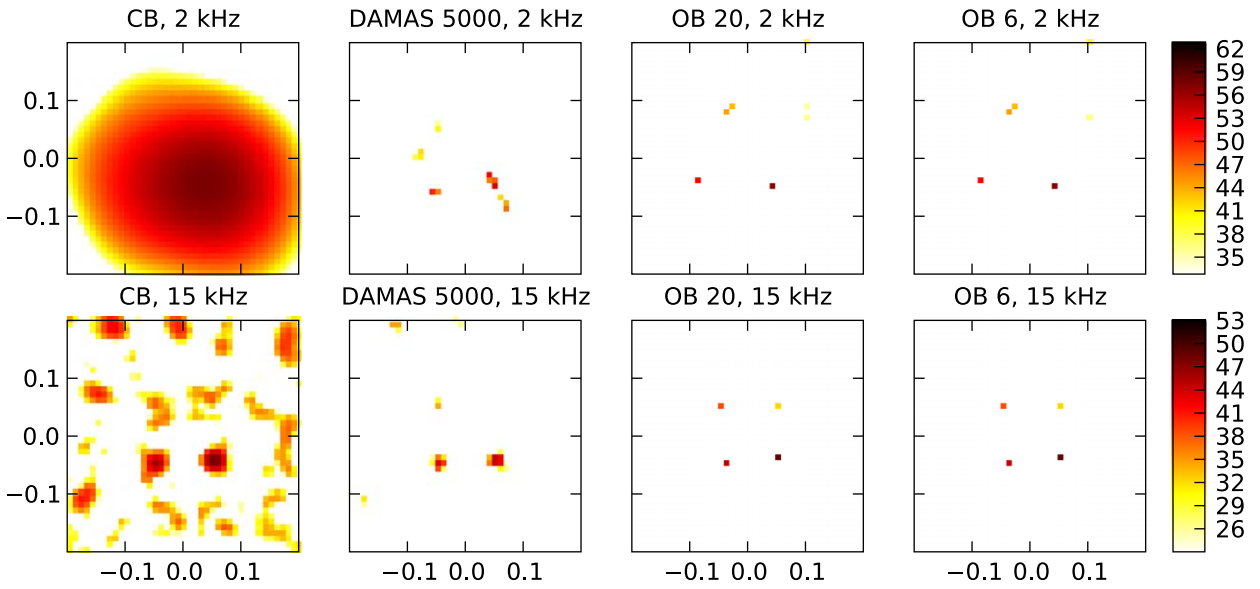


**Fig. 7.** Maps of sound pressure level as in Fig. 5, but for configuration 3 from Table 1.

The second test configuration result in Figs. 8(c) and (d) is different: The estimates of the spectrum of the source with highest level is practically the same for DAMAS and OB over the whole frequency range. For the other sources this holds only above 2 kHz. For lower frequencies, OB fails to produce a result at all and the DAMAS estimate of the spectra is incomplete. The results for the third test configuration in Figs. 8(e) and (f) are similar with the exception of the two weakest sources, where DAMAS underestimates the source level.

A quantitative comparison of OB and DAMAS for the four loudspeaker experiment is possible by comparing the respective results with the benchmark configuration 4. In this configuration only loudspeaker A was present as a single source. In Table 2, the sound pressure levels relative to the benchmark are given for all loudspeakers and configurations as the sum of the third-octave band levels from 2 to 20 kHz. For both algorithms, the deviation from the desired results is in most cases less than 1 dB. The difference between the individual OB and DAMAS results is always less than 1 dB. Again, this is true with the exception of DAMAS and the loudspeaker D in the third test case.

The maps, the spectra and the comparison of the measured levels allow to assess the quality of the OB results. In the case of the four loudspeaker laboratory setup these results have generally a quality similar to those from DAMAS. One exception is the low frequency range where the precision of both the location and the level of the sources is less precise. Here, DAMAS has the advantage of a more accurate source localization. One advantage of the proposed OB algorithm is the more robust behavior with weak sources.

A final test using the results from the four loudspeaker setup concerns the influence of additional noise that may be present in a measurement. To simulate additional noise, white noise signals were added to every microphone signal from the measurement on the third test configuration. The white noise signals had an RMS amplitude of 3 dB below the RMS amplitude of the original microphone signal. Thus, considerable additional noise was present in the resulting signals with a signal-to-noise ratio of 3 dB. The results of OB and DAMAS using the noisy signals are shown in Fig. 9. Differences are notable in the OB results only for the weaker sources in the high frequency range. Even though the weakest of the four sources has an amplitude well below that of the noise, the influence of the noise on the result remains small. For DAMAS, the result is practically unaltered. However, the weakest source is not detected at all for some frequency bands.

### 4.3. *Airfoil trailing edge noise*

Acoustic testing of configurations in a wind tunnel is a frequent application of microphone arrays. Thus, the proposed method is examined here regarding its performance for a typical wind tunnel experiment. The trailing edge noise measurements for the SD 7003 airfoil experiment detailed in Section 3 and Fig. 2 were analyzed. In these measurements the array is located outside the flow and the sound must travel from a potential source at the trailing edge through the flow inside the jet, through the shear layer and then through a large region without flow before it reaches the array microphones. In such a setup, the sound is convected by the flow and refracted by the shear layer of the jet. A number of methods for the correction of the shear layer is available (e.g. [3,29,37]). However, for the results reported here no shear layer correction has been applied, because the conical and deflected shape of the shear layer does not agree very well with available correction models. In prior tests the impact of shear layer corrections on the source localization was found to be relatively small for the described wind tunnel and the wind speed used.

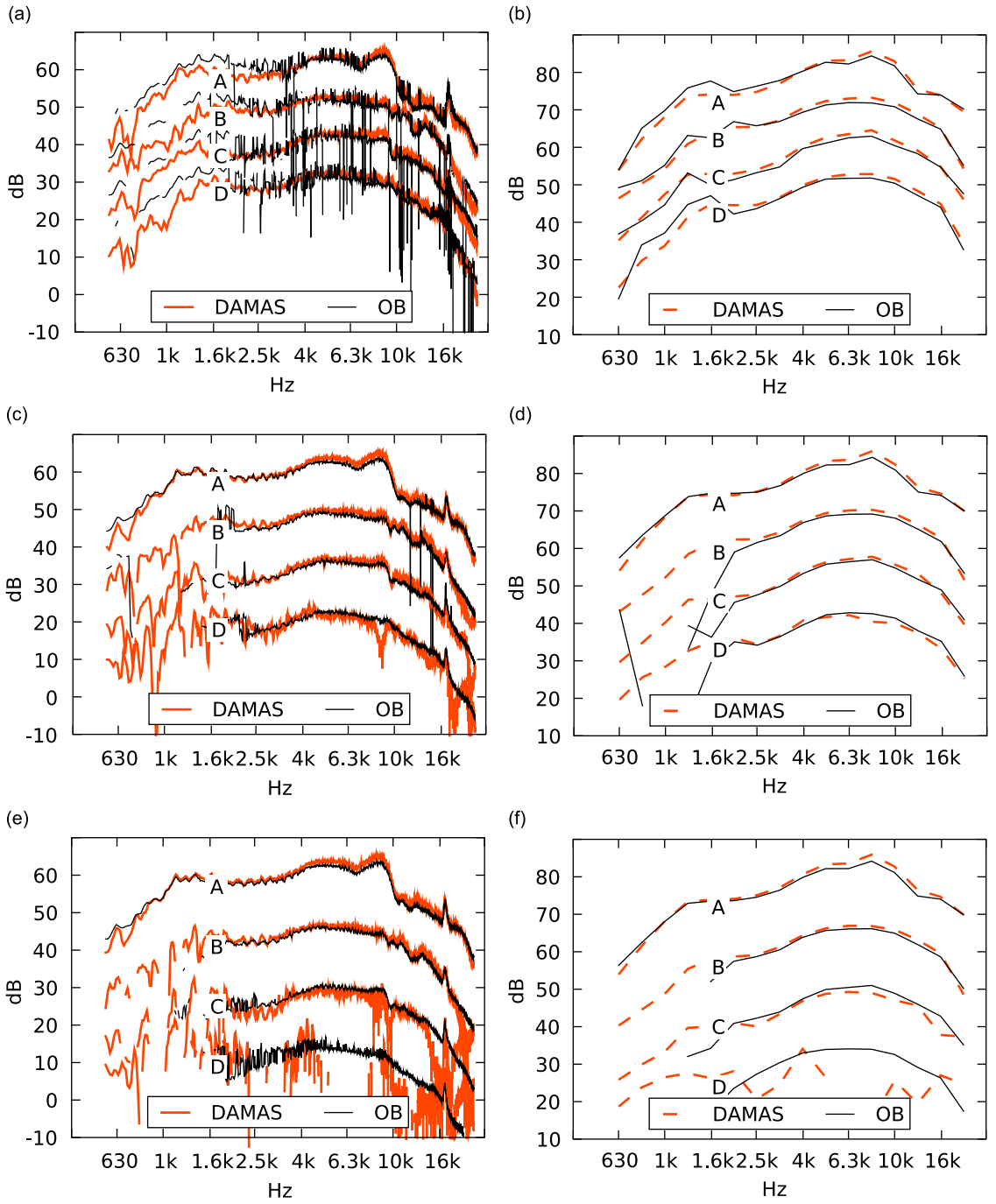


**Fig. 8.** Sound pressure level in the array center, narrow band spectra (a,c,e) and third octave spectra (b,d,f), orthogonal beamforming (OB) compared to DAMAS deconvolution, the spectra for the sources B, C and D are shifted for clarity of presentation by −10, −20 and −30 dB, respectively, (a) and (b): configuration 1, $\Delta L = 0$ dB, (c) and (d): configuration 2, $\Delta L = 3$ dB, (e) and (f): configuration 3, $\Delta L = 6$ dB.

As the number of sources is not known prior to the experiment, the number of eigenvalues to include in the OB processing must be guessed. It was obvious from the four loudspeaker experiment that it is not harmful to include more eigenvalues than needed. Thus, again the 20 highest eigenvalues were used. From results not reported here it was also found that the inclusion of the full set of eigenvalues did not alter the results considerably and led only to higher computational effort. A second OB calculation was done with the six highest eigenvalues only. This number deliberately underestimates the number of sources and should lead to different results. Again, the OB results are compared with CB using diagonal removal and DAMAS with 5000 iterations is used as a benchmark.

**Table 2**
Test configurations: loudspeaker driving signal levels and measured sound pressure levels of all loudspeakers relative to benchmark (configuration 4) for the frequency range 2–20 kHz.

| Configuration | $L_A$ (dB) | $L_B$ (dB) | $L_C$ (dB) | $L_D$ (dB) |
|---|---|---|---|---|
| 1, signal level | 0.0 | 0.0 | 0.0 | 0.0 |
| 1, DAMAS | 0.2 | −0.4 | −0.2 | −0.8 |
| 1, OB | 0.2 | −1.0 | −1.0 | −1.1 |
| 2, signal level | 0.0 | −3.0 | −6.0 | −9.0 |
| 2, DAMAS | 0.5 | −3.2 | −6.5 | −11.0 |
| 2, OB | −0.3 | −4.1 | −7.0 | −10.7 |
| 3, signal level | 0.0 | −6.0 | −12.0 | −18.0 |
| 3, DAMAS | 0.5 | −6.5 | −14.0 | −23.6 |
| 3, OB | −0.5 | −7.1 | −12.9 | −19.0 |
| 4, signal level | 0.0 | – | – | – |
| 4, DAMAS | 0.0 | – | – | – |
| 4, OB | 0.0 | – | – | – |

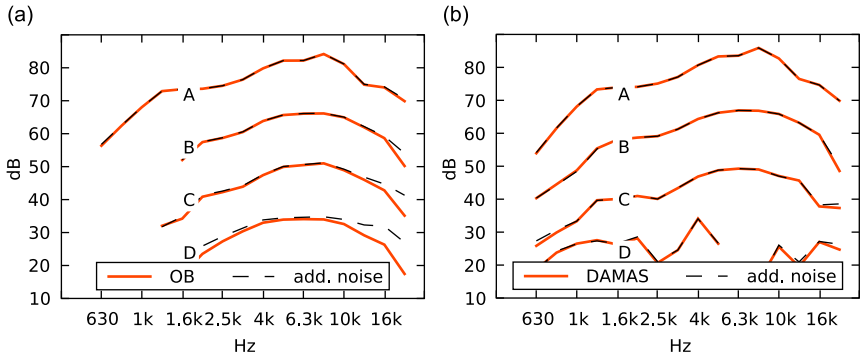


**Fig. 9.** Sound pressure level in the array center for configuration 3, original results compared to results when additional noise is present in the microphone signals, the spectra for the sources B, C and D are shifted for clarity of presentation by −10, −20 and −30 dB, respectively, (a): orthogonal beamforming (OB), (b): DAMAS deconvolution.

Fig. 10 shows the maps of sound pressure contribution for the five octave bands from 1 to 16 kHz. The CB results show the location of the trailing edge noise source, but suffer from low resolution at low frequencies and show deterioration by noise at higher frequencies. DAMAS performs quite robust, resolving the sound source location in all frequency bands. In the two lower octave bands the interaction of the shear layer with the trailing edge produces two sources that appear to have a level higher than that of the trailing edge noise produced by the flow in the core jet. For 4 kHz and above the center trailing edge is the main sound source. Two sources appear at the leading edge of the airfoil for 2 kHz and above. The noise originating from the wind tunnel nozzle is present in the DAMAS maps for 8 and 16 kHz. At these higher frequencies the deconvolution suffers from the deviation between theoretical and true point spread functions of the array. Consequently, the DAMAS map is somewhat degraded especially for the 16 kHz octave band.

The OB results for both 6 and 20 eigenvalues indicate that the source position is at the trailing edge for all octave bands. In contrast to the DAMAS results, the different sound sources at the trailing edge cannot be distinguished at low frequencies. This is probably due to the less precise estimate of source locations at low frequencies that could also be noted in the four loudspeaker results. The leading edge sources at higher frequencies can also be identified from both OB results. However, the noise from the wind tunnel nozzle appears only in the OB results that use 20 eigenvalues. It can also be noted that in the high frequency range the OB maps are generally less polluted with spurious sources than the DAMAS results.

From the maps the result quality can be estimated mainly in terms of the source localization. To allow a quantitative comparison, all results were integrated over the sector of the assumed location of the trailing edge noise source. While for DAMAS and OB this integration is straightforward, for CB the result was corrected for the main lobe with of the beamformer using the appropriate point spread function [1].

Fig. 11 shows the spectra that results from this integration. Because the focus of the proposed method is on quantitative estimation rather than on localization, the DAMAS benchmark is calculated from beamforming with diagonal removal as well as with the full cross spectral matrix. While the diagonal removal provides the best localization, source levels may be underestimated [12]. The result with full cross spectral matrix does not underestimate the source levels, but may contain

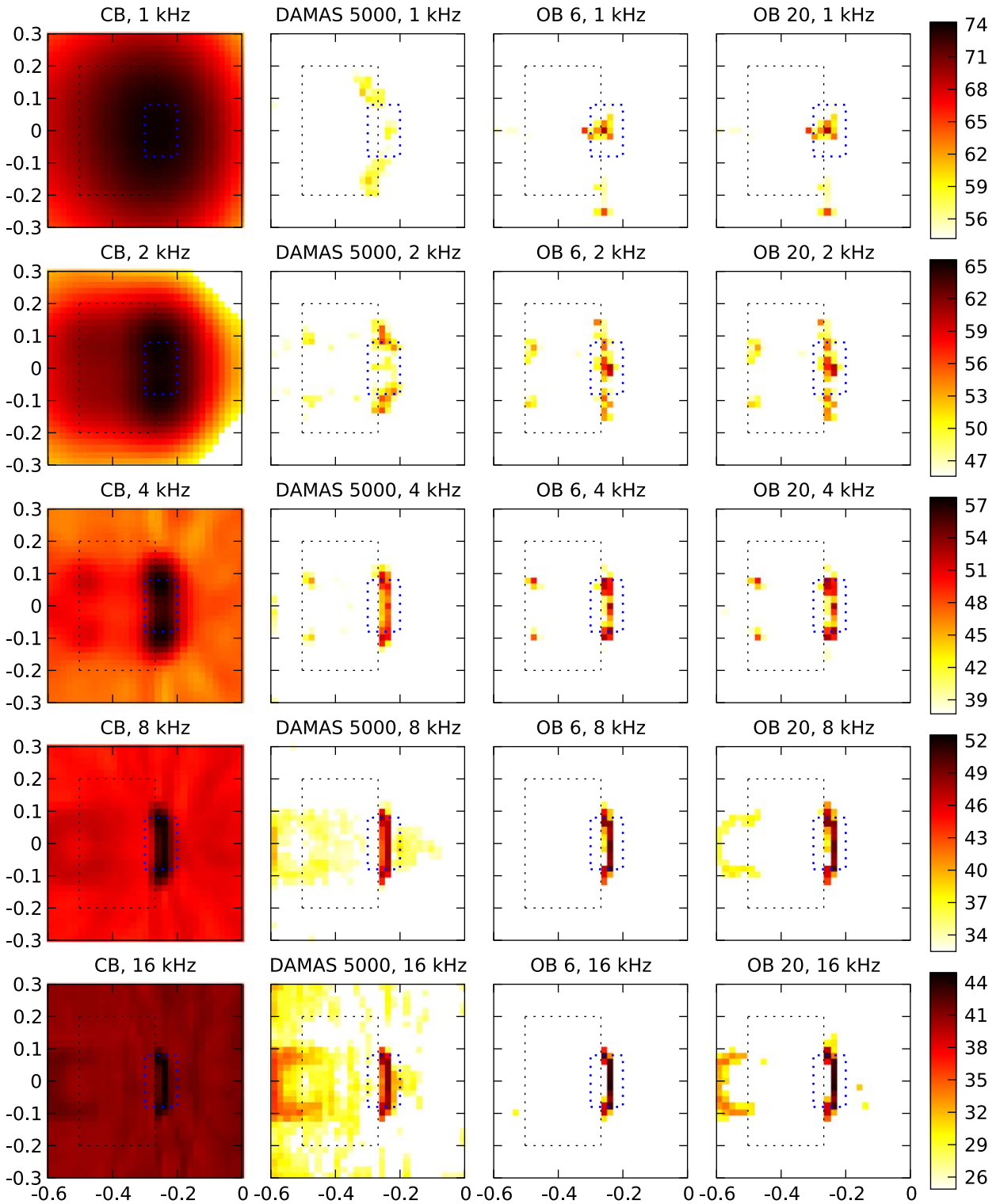


**Fig. 10.** Maps of sound pressure level in dB in the distance of 0.68 m from the trailing edge of an SD7003 airfoil, dimensions are in m, results from conventional beamforming (CB), the deconvolution approach for the mapping of acoustic sources (DAMAS) using 5000 iterations and orthogonal beamforming (OB) using the 6 and the 20 largest eigenvalues, dotted lines mark the airfoil and the trailing edge noise sector shown in Fig. 2.

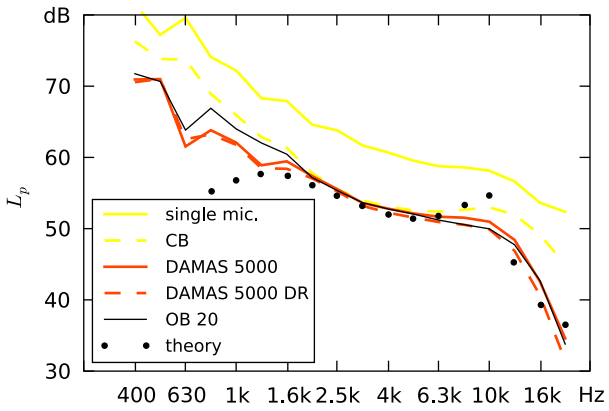


**Fig. 11.** Third octave sound pressure level of trailing edge noise of an SD 7003 airfoil with a chord length of 235 mm in a distance of 0.68 m perpendicular to chord and trailing edge, at $U_\infty = 52$ m/s, comparison of single microphone results, conventional beamforming (CB), orthogonal beamforming (OB), DAMAS deconvolution with full cross spectral matrix and with prior diagonal removal (DR) and theoretical prediction.

**Table 3**
Computational effort for different algorithms: number of real-valued floating point multiplications (flop count) for one frequency, timing for 1.8 GHz personal computer ($N = 56$, $L = 1681$) with calculation of steering vectors included and calculation of point spread functions for DAMAS excluded.

| Algorithm | CB | DAMAS | OB | |
|---|---|---|---|---|
| Parameters | | $K = 100$ | $M = 6$ | $M = 20$ |
| Flop count | $4(N^2+N)L$ | $4(N^2+N)L+KL^2$ | $(8N+1)ML$ | |
| | $2.1 \times 10^7$ | $3.0 \times 10^8$ | $4.5 \times 10^6$ | $1.5 \times 10^7$ |
| Time (s) | 0.09 | 1.61 | 0.06 | 0.09 |

contributions from additional noise. Assuming that the deconvolution itself works properly and converges, the correct result should therefore be bounded by the two DAMAS results. This is the case for the OB result in the high frequency range above 2 kHz. Moreover, even down to 1 kHz, where OB provides no accurate source localization, the deviation between the DAMAS and the OB results is less than 2 dB. The CB result that is also show in Fig. 11 agrees with OB and DAMAS in the medium frequency range, but gives considerably higher levels for both low and high frequencies.

Brooks et al. [38] derived a method for the prediction of airfoil trailing edge noise. In this method, the trailing edge noise is predicted from the boundary layer displacement thickness on either side of the airfoil, which in turn is predicted using empirical formulas. In addition, the vortex shedding at the blunt trailing edge is taken into account. Both OB and DAMAS show reasonable agreement with this prediction in the frequency range above 1 kHz. For comparison, Fig. 11 includes also the result from the single array microphone that is situated closest to the trailing edge. This approach uses no beamforming or similar method at all. Consequently, any additional noise and noise from other sources is included and source levels are overestimated.

### 4.4. Computational requirements

Especially when a large number of measurements is to be analyzed, the calculation time is of importance. A measure for this time is the number of floating point multiplications per frequency that have to be performed. For CB this number depends on the number of microphones and on the number $L$ of grid points in the beamforming map. Additionally, the number of sources considered and the number of iterations $K$ have an influence for OB and DAMAS, respectively.

The CB, DAMAS and OB algorithms have considerably different computational requirements. Table 3 gives an overview of the computational effort for the three algorithms. The expressions for the number of multiplications for CB, DAMAS and OB are based on (13), (14) and (29), respectively. In the case of OB, it is of advantage that no full cross spectral matrix need to be used for the multiplication in (30), but only a dot product of the steering vector and the eigenvector. The estimated number for DAMAS is multiplied by the number of iterations. For OB, it is multiplied by the number of sources that were considered. Any complex multiplication is counted as four real-valued multiplications. Other necessary operations such as the calculation of the steering vectors and comparison operations that are necessary to find the maximum in the beamforming map are neglected, though they may need considerable time in a practical implementation. This is especially true for DAMAS, where the calculation of the point spread function may be more expensive than the DAMAS iteration process itself.

The comparison shows that OB needs much less multiplication operations than DAMAS and, depending on the number of sources considered, even less than CB. The computational time on an 1.8 GHz personal computer also shown in Table 3 is much less for OB than that for DAMAS. Other fast deconvolution methods [11,15] need less computational time than DAMAS, but require prior beamforming in any case. Consequently, these methods also need more computational time than OB.

### 4.5. Advantages and limitations of the proposed method

The proposed method has the major advantage to offer very fast processing compared to any other method that bases on microphone array beamforming. This is a limited benefit if only a few number of measurements are to be processed. However, with a larger number of measurements this becomes important and enables the prompt processing of the data from several thousand measurements [39]. Another field of application that demands very fast processing is beamforming using very large map grids. Such scenario may arise when the grid extends in three dimensions [40].

Another property of the method may be of advantage in certain cases. The result is recovered from the eigenvalues of the cross spectral matrix of microphone signals. The sum of the eigenvalues equals the trace of that matrix, which is the sum of all autospectra. Thus, the result of the method will never exceed the result that would be constructed from the autospectra of the microphones without any beamforming. This limit for the result is especially important in environments with strong reflections. Reflections result in correlated mirror sources and consequently the beamforming map shows both true sources and mirror sources. The conventional integration over sectors of the map may include additional contributions from the mirror sources and may thus overestimate the source level.

Similar to most beamforming and deconvolution methods, the source localization with OB also rests on the assumption of uncorrelated point sources. However, in practice multiple correlated point sources or locally distributed coherent sources may be present. In this case, the assumption that the highest peak in a beamforming map coincides with the source locations is not necessarily true. Thus, OB may fail to detect the location of some of these sources. However, the estimation of source strengths is solely based on the eigenvalues and needs the assumption of uncorrelated sources only for the correct assignment to source locations.

Additional noise was already considered in the derivation of the method. Under certain circumstances, such non-acoustic noise may be very strong, e.g. from flow boundary layer pressure fluctuations when the microphone array is placed in the flow for measurements in closed test sections in wind tunnels. As it can be seen from the example in Fig. 9 the influence on the OB result remains very small even if the noise exceeds the source signal considerably. A more severe limitation arises from strong unwanted sources that are not located inside the map grid. In this case, the highest peak found in the map for an eigenvalue that corresponds to such a source is not the location of the source. The OB algorithm will then assume that there is a strong source inside the map, usually near the edge of the map. However, this problem can be mitigated in practice if the map grid is somewhat enlarged and the margins of the map are not considered in the final result.

## 5. Conclusion

In this paper, a new method for processing microphone array measurements has been proposed. This method makes use of an eigenvalue decomposition of the cross spectral matrix of microphone signals with subsequent beamforming for each component of the cross spectral matrix. The maximum in each beamforming map indicates the position of one source, while the appropriate eigenvalue is taken as an approximation for the source strength. The quality of this approximation depends on the frequency and on the level difference between individual sources.

Two different experimental setups, a laboratory setup of four loudspeakers and an airfoil trailing edge noise experiment in an aeroacoustic wind tunnel, were used for the practical application of the method. The DAMAS approach was used as a benchmark for the results. The proposed method shows comparable performance in the estimation of quantitative source spectra over a wide range of frequencies. In particular, it works well for weak sources and also in the presence of additional noise in the microphone signals. For low frequencies, the performance degrades because of inaccurate source localization. The main advantage of the method is its computational efficiency. The computational requirements of the method are similar to those for conventional beamforming, by far less than that of DAMAS and also less than that of other deconvolution methods.

## Acknowledgements

The author is indebted to Christoph Fritzsche and Thomas Geyer for their help with the experiments.

## References

[1] T. Brooks, W. Humphreys, Effect of directional array size on the measurement of airframe noise components, AIAA paper 99-1958, 1999.
[2] M. Mosher, M.E. Watts, M. Barnes, J. Bardina, Microphone array phased processing system (MAPPS): phased array system for acoustic measurements in a wind tunnel, SAE paper 1999-01-5576, 1999.

[3] R. Dougherty, Beamforming in acoustic testing, in: T. Mueller (Ed.), *Aeroacoustic Measurements*, Springer, Berlin, Heidelberg, Germany, 2002, pp. 62–97.
[4] S. Oerlemans, P. Sijtsma, Determination of absolute levels from phased array measurements using spatial source coherence, Technical Report NLR-TP-2002-226, National Aerospace Laboratory NLR, 2002.
[5] J. Hald, Combined NAH and beamforming using the same array, *B&K Technical Review* 1 (2005) 11–39.
[6] D. Blacodon, G. Elias, Level estimation of extended acoustic sources using a parametric method, *Journal of Aircraft* 41 (2004) 1360–1369.
[7] U. Michel, S. Funke, Noise source analysis of an aeroengine with a new inverse method sodix, AIAA paper 2008-2860, 2008.
[8] T.F. Brooks, W.M. Humphreys, A deconvolution approach for the mapping of acoustic sources (DAMAS) determined from phased microphone arrays, AIAA paper 2004-2954, 2004.
[9] T.F. Brooks, W.M. Humphreys, Extension of damas phased array processing for spatial coherence determination (damas-c), AIAA paper 2006-2654, 2006.
[10] R. Dougherty, Extensions of DAMAS and benefits and limitations of deconvolution in beamforming, AIAA paper 2005-2961, 2005.
[11] K. Ehrenfried, L. Koop, Comparison of iterative deconvolution algorithms for the mapping of acoustic sources, *AIAA Journal* 45 (7) (2007) 1584–1595.
[12] T. Yardibi, J. Li, P. Stoica, L. Cattafesta III, Sparsity constrained deconvolution approaches for acoustic source mapping, *The Journal of the Acoustical Society of America* 123 (2008) 2631.
[13] R.P. Dougherty, R.W. Stoker, Sidelobe suppression for phased array aeroacoustic measurements, AIAA paper 98-2242, 1998.
[14] Y. Wang, J. Li, P. Stoica, M. Sheplak, T. Nishida, Wideband RELAX and wideband CLEAN for aeroacoustic imaging, *The Journal of the Acoustical Society of America* 115 (2004) 757.
[15] P. Sijtsma, CLEAN based on spatial source coherence, AIAA paper 2007-3436, 2007.
[16] B. Van Veen, K. Buckley, Beamforming: a versatile approach to spatial filtering, *IEEE Signal Processing Magazine* 5 (2) (1988) 4–24.
[17] H. Krim, M. Viberg, Two decades of array signal processing research, the parametric approach, *IEEE Signal Processing Magazine* (1996) 67–94.
[18] R. Roy, A. Paulraj, T. Kailath, ESPRIT—a subspace rotation approach to estimation of parameters of cisoids in noise, *IEEE Transactions on Acoustics, Speech and Signal Processing* 34 (5) (1986) 1340–1342.
[19] J. Capon, High-resolution frequency-wavenumber spectrum analysis, *Proceedings of the IEEE* 57 (8) (1969) 1408–1418.
[20] J. Li, P. Stoica, Z. Wang, On robust capon beamforming and diagonal loading, *IEEE Transactions on Signal Processing* 51 (7) (2003) 1702–1715.
[21] R.A. Gramann, J.W. Mocio, Aeroacoustic measurements in wind tunnels using adaptive beamforming methods, *The Journal of the Acoustical Society of America* 97 (1995) 3694–3701.
[22] D. Long, Acoustic source location in wind tunnel tests via subspace beamforming, AIAA paper 2003-369, 2003.
[23] Z. Wang, J. Li, P. Stoica, T. Nishida, M. Sheplak, Constant-beamwidth and constant-powerwidth wideband robust Capon beamformers for acoustic imaging, *The Journal of the Acoustical Society of America* 116 (2004) 1621.
[24] R. Schmidt, Multiple emitter location and signal parameter estimation, *IEEE Transactions on Antennas and Propagation* 34 (3) (1986) 276–280.
[25] W. Liggett Jr., Passive sonar processing for noise with unknown covariance structure, *The Journal of the Acoustical Society of America* 51 (1972) 24.
[26] G. Su, M. Morf, Signal subspace approach for multiple wide-band emitter location, *IEEE Transactions on Acoustics, Speech and Signal Processing* 31 (6) (1983) 1502–1522.
[27] T. Suzuki, Identification of multipole noise sources in low mach number jets near the peak frequency, *The Journal of the Acoustical Society of America* 119 (2006) 3649.
[28] T. Suzuki, Generalized inverse beam-forming algorithm resolving coherent/incoherent, distributed and multipole sources, AIAA paper 2008-2954, 2008.
[29] R. Amiet, Refraction of sound by a shear layer, AIAA paper 1977-54, 1977.
[30] J. Gentle, *Matrix Algebra*, Springer, New York, 2007.
[31] P. Stoica, R. Moses, *Introduction to Spectral Analysis*, Prentice-Hall, Upper Saddle River, NY, 1997.
[32] S. Gershgorin, Ueber die Abgrenzung der Eigenwerte einer Matrix, *Izvestiya akademii nauk USSR otdeleniya fiziko-matematicheskikh nauk* 7 (1931) 749–754.
[33] R. Horn, C. Johnson, *Matrix Analysis*, Cambridge University Press, Cambridge, 1990.
[34] W.M. Humphreys, T.F. Brooks, W.W. Hunter, K.R. Meadows, Design and use of microphone directional arrays for aeroacoustic measurements, AIAA paper 98-0471, 1998.
[35] M. Wax, T. Kailath, Detection of signals by information theoretic criteria, *IEEE Transactions on Acoustics, Speech and Signal Processing* 33 (2) (1985) 387–392.
[36] E. Sarradj, C. Fritzsche, T. Geyer, J. Giesler, Acoustic and aerodynamic design and characterization of a small-scale aeroacoustic wind tunnel, *Applied Acoustics* 70 (2009) 1073–108010.1016/j.apacoust.2009.02.009.
[37] P. Soderman, C. Allen, Microphone measurements in and out of airstream, in: T. Mueller (Ed.), *Aeroacoustic Measurements*, Springer, Berlin, Heidelberg, Germany, 2002, pp. 62–97.
[38] T.F. Brooks, D.S. Pope, M.A. Marcolini, Airfoil self-noise and prediction, NASA reference publication 1218, 1989.
[39] T. Geyer, E. Sarradj, C. Fritzsche, Measurement of the noise generation at the trailing edge of porous airfoils, Experiments in Fluids (2009), doi:10.1007/S00348-009-0739-X.
[40] T. Brooks, W. Humphreys, Three-dimensional application of DAMAS methodology for aeroacoustic noise source definition, AIAA paper 2005-2960, 2005.